Available on CMS information server

CMS CR -2020/051

The Compact Muon Solenoid Experiment

Conference Report

Mailing address: CMS CERN, CH-1211 GENEVA 23, Switzerland

10 February 2020

Study of Interpad-gap of FBK (UFSD3) and HPK 3.1 Type sensors with Transient Current Technique

Shudhashil Bharthuar for the CMS Collaboration

Abstract

The Phase-II upgrade of LHC to HL-LHC by 2026 allows an increase in the operational luminosity
value by a factor of 5-7 that will result in delivering 3000 fb^{-}1ormoreintegratedluminosity.Thisamountofdatawillnotjustal
200.Tocopewithhighpileuprates, precisiontimingdetector(MTD)thatwillmeasureminimumionizingparticles(MIPs)
40psandhermeticcoverageuptoapseudo−rapidityofIetaI = 3isproposedbytheCMSexperiment.Anendcappart(1.6ltIet
gainavalanchedetector(LGAD)technology.ThethirdproductionofUltraFastSiliconDetectors(UFSD3)fromFondazi
padgapwidthforbothsensortypeshasbeencarriedout.Resultsofmeasuredinter−padgapwidthsandspatialmappingswith
activeregionsusingMIPs(IRlight)fromtheScanning−TransientCurrentTechnique(Scanning−
TCT)set−upwillbeshown.Afill−factor, whichistheratiooftheareawithintheactiveregion(Gainregion)totheareaofthe
factorvariesdependingontemperature(from25Cto−25C)andprotonfluenceonirradiationwillalsobeshown.

Presented at *HSTD12 12th International Hiroshima Symposium on the Development and Application of Semiconductor Tracking Detectors (HSTD12)*

Study of Interpad-gap of HPK 3.1 production LGADs with Transient Current Technique*

S. Bharthuar[a,b,], J. Ott[a,d], K. Helariutta[c], V. Litichevskyi[a,b], E. Brücken[a,b], P. Luukka[a,e]

[a]*Helsinki Institute of Physics, Gustaf Hällströmin katu 2, 00014 University of Helsinki, Finland*
[b]*Department of Physics, Gustaf Hällströmin katu 2, 00014 University of Helsinki, Finland*
[c]*Department of Chemistry, Gustaf Hällströmin katu 1, 00560 University of Helsinki, Finland*
[d]*Aalto University, Department of Electronics and Nanoengineering, Tietotie 3, Espoo, FI-02150, Finland*
[e]*Lappeenranta University of Technology, Skinnarilankatu 34, 53850 Lappeenranta, Finland*

Abstract

The Phase-II upgrade of the Large Hadron Collider (LHC) to High-Luminosity LHC (HL-LHC) allows an increase in the operational luminosity value by a factor of 5–7 that will result in delivering 3000 fb^{-1} or more integrated luminosity. To achieve high luminosity, the number of interactions per bunch crossings (pileup) will increase up to a value of 140–200. To cope with high pileup rates, precision minimum ionizing particles (MIPs) timing detector (MTD) with a time resolution of ∼30–40 ps and hermetic coverage up to a pseudo-rapidity of $|\eta| = 3$ is proposed by the Compact Muon Solenoid (CMS) experiment. An endcap part ($1.6 < |\eta| < 3$) of the MTD, called the endcap timing layer, will be based on low-gain avalanche detector (LGAD) technology. The 3.1 production of LGADs from Hamamatsu Photonics K.K. (HPK) include 2x2 sensors with different structural strategies, in particular, different nominal values of narrower inactive region widths between the pads. These sensors have been designed to study their fill factor, which is the ratio of the area within the active region (gain region) to the total sensor area. A comparative study on the dependence of breakdown voltage with the interpad-gap width for the sensors has been carried out. Using MIPs (infrared light) from the Scanning-Transient Current Technique (Scanning-TCT) set-up show that the fill factor does not vary significantly with a variation in temperature and at high proton fluence irradiation.

Keywords: Low Gain Avalanche Detector (LGAD), Scanning-TCT, Fill Factor

---

Email address: `shudhashil.bharthuar@helsinki.fi` (S. Bharthuar)
[1]On behalf of the CMS Collaboration

1. Introduction

The High Luminosity Large Hadron Collider (HL-LHC) era, also known as the Phase-2 operation of the LHC, will be functional after Long Shutdown 3 (LS3). During the HL-LHC phase, the number of interactions per bunch crossings will increase to an average value of 140 corresponding to a nominal luminosity of 5.0×10^{34} cm^{-2}s^{-1}. Ultimately, the luminosity will be leveled up to a nominal value of 7.5×10^{34} cm^{-2}s^{-1}, at the cost of producing 200 interactions per each bunch crossing. The amount of collected data corresponding to an integrated luminosity of 3000 fb^{-1}, will increase the precision of the Standard Model (SM) measurements and the sensitivity for Beyond Standard Model (BSM) searches [1]. Due to additional beam collisions, spatial overlapping of the tracks and energy deposition will cause a degradation in the particle identification and reconstruction of the tracks during the hard interaction. In addition, the radiation damage caused due to the high collision rate integrated over time can not be tolerated by the existing detectors. Therefore, the upgraded detector must be able to survive and function efficiently in the radiation harsh environment. It should also be able to mitigate the problem of high pileup rates by transporting a much higher rate of data off the detector to be recorded for analysis.

In the upgrade plan for the HL-LHC era, the Compact Muon Solenoid (CMS) experiment will install a precision minimum ionizing particles timing detector (MTD) to measure minimum ionizing particles (MIPs) with a time resolution of nearly 30-40 ps, degrading slowly to a magnitude of 50-60 ps due to radiation damage. The MTD will allow time of arrival (ToA) measurements that can separate the collisions very close in space as well as in time with a hermetic angular coverage up to a pseudo-rapidity of $|\eta| = 3$ [2].

The MTD will be a thin layer between the tracker and the electromagnetic calorimeter of the CMS experiment. It will consist of a barrel ($|\eta|$ <1.5) and an endcap part (1.6 <$|\eta|$< 3). The endcap part of the MTD, known as the endcap timing layer (ETL), will be based on low gain avalanche detector (LGAD) technology. The timing resolution and performance of the ETL depends upon the optimal design of the sensors which can be achieved when each of the hits as particles cross the two silicon layers have high gain, low noise and uniform response. These objectives can be achieved by studying and optimising some of the crucial features of the LGADs, which are: fill factor, wafer uniformity, quality of multi-pad sensors, single pad leakage current, hit efficiency and signal uniformity, gain and noise, long term stability and time resolution [3].

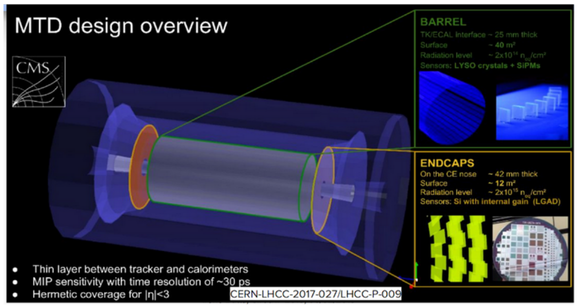

Figure 1: CMS MTD design layout showing the positioning of its barrel and endcap part [4]

In this report, the authors have focused on the study of fill factor which is the ratio of the active area and the total sensor area. This value can be less than 100% due to the edge width and the no-gain region between the pads. The fill factor depends upon the nominal distance between adjacent pads of the sensors, known as the interpad-gap. Further, the breakdown voltage of the sensors depends upon the design of the gain termination region which is affected with the nominal interpad-gap value.

The 3.1 production batch LGADs provided by one of the competitive vendors, Hamamatsu (HPK), have been studied in this report. The specification of the samples have been mentioned in Section 2. I-V characterisation of the sensors (shown in Section 3.1) with varying interpad-gaps shows how the breakdown voltage depends upon the inaction region width. Further, since the gain of these sensors depends upon temperature and proton fluence of irradiation, the interpad-gap and fill factor have been studied with these varying factors by using the Scanning Transient Current Technique (TCT) set-up (shown in Section 3.2).

2. Samples Measured

The samples measured are sensors from HPK 3.1 production batch. The design of the sensors studied are according to 2019 CMS MTD Technical Proposal (TP) [2]. The thickness of the active p-type bulk region of the sensors is of a magnitude of 50 µm. The sensors have four pads (2×2) with a common guard ring around them. Each of the pads has an area of 1×3 mm^2. The difference in the samples is the distance between the adjacent pads, called interpad-gap. The nominal values of interpad-gap are 30 µm, 50 µm, 70 µm and 95 µm, respectively. The sensors have been categorised into two types: Type A and Type B on the basis of their structural prototypes (as shown in Figure 2).

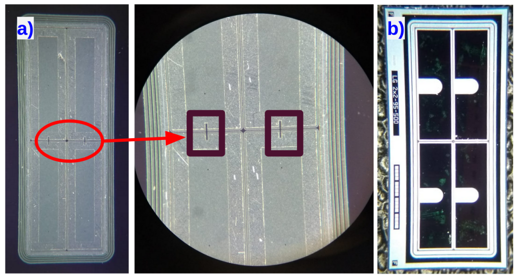

Figure 2: HPK 3.1 production sample with 2×2 sensor showing sensors a) with broader metallisation region on pads and small optical opening running across adjacent pads (Type A) and b) individual pads with wider optical opening (Type B).

3. Measurements

3.1. IV-CV Measurements

Capacitance versus Voltage (C-V) and Current versus Voltage (I-V) measurements were performed at the probe station in the Detector Laboratory in Helsinki Institute of Physics (HIP), Finland. Capacitance^{-2} versus Voltage plot from C-V measurements shows that the full depletion voltage of the sensors is of a magnitude of 50 V.

I-V measurements of sensors with varying nominal interpad-gaps were performed in two different modes depending upon the floating/grounding configuration of the remaining pads while current was readout from one of the pads (shown in Figure 3). The sensors have a breakdown voltage of 220 V. The breakdown voltage is independent of the floating and/or grounding configuration of the remaining pads for sensors with 50 µm, 70 µm and 95 µm nominal interpad-gap; but is not the same for the ones with 30 μm nominal interpad-gap (shown in Figure 3a and 3b). This shows that the breakdown voltage is dependent upon the design of the gain termination region and the nominal value of interpad-gap.

3.2. Scanning-Transient Current Technique Measurements

TCT is a method commonly used for electrical characterisation of semiconductor detectors. The measurements in this study were performed by Particulars (Ljubljana, Slovenia) based Scanning-TCT setup [5]. Optical excitation was performed with an infrared (IR) laser ($\lambda = 1064\,\text{nm}$) directed on the optical opening in front plane of the sensor. The measurements were performed at low a laser intensity of 62.5 %, equivalent to 4-5 MIPs, in order to study the effect due to the gain layer. The bias voltage is applied to the back plane of the sensor while the transient signal is read from the front. The laser illumination generates charge carriers within the bulk of

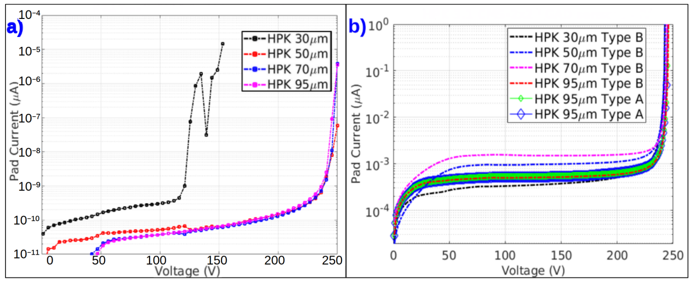

Figure 3: Current versus voltage plots of HPK 3.1 sensors wherein: a) Current is readout from one the pads while the three pads are left floating. Guard ring is grounded. b) Current is readout from one of the pads, while the other pads as well as the guard ring are grounded. Note: All the plots are in logarithmic scale.

the active depleted region. Since the sensors have a p-type bulk, under reverse-bias mode, the transient signal is due to the electrons that are quickly gathered to the front-end electrode. Therefore, the resulting signal read out by an oscilloscope is a fast signal of 2.5 ns width.

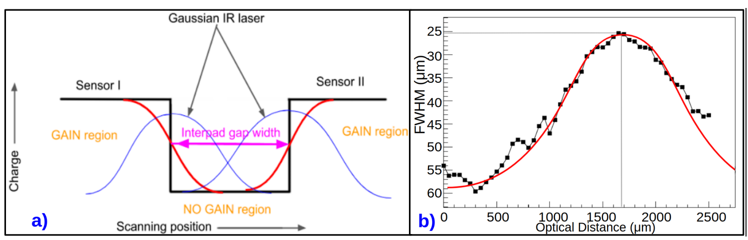

Figure 4: a) Measured interpad-gap is the distance between the mid-point of the S-curves of adjacent sensors. b) FWHM vs Optical distance of the IR laser from sensor. Gaussian shape IR spot with size: 25 µm. Focus position of the laser: 1650 µm.

In addition to the IR laser, the other components in measurement setup were a focusing optics, a sample holder mounted on a XYZ stage for scanning the entire surface of the detector, a Keithley 2410 1100 V Sourcemeter unit, 180 V (maximum allowance) Bias-Tee, a wide band current amplifier with a Tenma power supply, a LeCroy WaveRunner 8404M-MS 4 GHz oscilloscope and a PC and DAQ with LAB-view based software. The repetition rate of the laser is adjustable from 5 kHz to 500 kHz. During the measurements, more than one hundred waveforms were recorded while scanning the laser illumination through the optical opening across two adjacent pads. The laser pulse was transmitted to the detector by an optical fiber. On performing a focus scan, the size of the Gaussian laser spot was determined to be of a magnitude of 25 µm (shown in Figure 4 b). The interpad profile observed in TCT scan is a convolution of step function and the Gaussian beam of IR laser: S-curve (as shown in Figure 4 a). The curve fitting function is an error-function of the form

$$f(x) = a + \left[\frac{b}{2} \times \mathrm{erf}\left\{\frac{\sqrt{2}(x-c)}{d}\right\}\right] \tag{1}$$

The step ends (= gain layer ends) at 50% of the convoluted function. This 50% value of the convoluted function (S-curve) is determined by parameter c of equation (1) . We compute the measured interpad-gap width as the distance between the 50% amplitude points of the two interpad profiles (i.e. the distance between 2 gain layers) of adjacent pads [2].

3.2.1. Measured interpad-gap with varying temperature:

The study on temperature dependence on the internal gain of LGADs plays an important role in the sensor performance due to its impact ionisation rate which is inversely proportional to the mean free path of the carriers [6]. Since the impact ionisation of the sensors depends on temperature, a proper understanding of the LGAD functionality with temperature variation is crucial as the gain affects the time resolution as well as the breakdown voltage of the detector [7].

Since the gain increases with a decrease in temperature [7], the charge collected increases as the temperature decreases. Figure 5a shows the pulse shape and amplitude of the signals recorded by the LeCroy oscilloscope as the laser is projected at the optical opening of one of the pads. The amplitude of the signal increases by a factor of 2.5 as the temperature is decreased from 25°C to -25°C. This is coherent to the increase in the charge collected due to the gain layer as the laser is projected at the optical opening of the sensor. The normalised value of collected charge increases by a factor of 2.8 as the temperature decreases from 25°C to -25°C [8].

The interpad-gap as well the leakage current were measured with temperature variation from 25°C to -25°C at a constant bias voltage of 180 V (shown in Figure 5). As expected, the leakage current value measured at a constant voltage of 180 V decreases by nearly an order of magnitude [8]. The measured interpad-gap values and the calculated fill factor of different sensors with varying nominal interpad-gaps have been tabulated in Table 1. It shows the percentage decrease in the interpad-gap as well as the variation in fill factor with varying temperature. The measured interpad-gap for the HPK 3.1 production sensors has an offset of approximately 40 µm from the the nominal value. This is coherent to the values measured at test beams in FNAL (measured at room temperature), mentioned in the MTD TDR 2019 [2]. The fill factor values measured at room temperature are also consistent with the measured fill factor provided in the MTD TDR 2019 [2].

HPK Sensor (nominal interpad-gap)	Measured Interpad-gap of sensor				Fill factor			
	At 25°C (in μm)	At 0°C (in μm)	At -25°C (in μm)	Decrease from 25°C to -25°C (in %)	At 25°C (in %)	At 0°C (in %)	At -25°C (in %)	Increase from 25°C to -25°C (in %)
30 µm	71.7	63.1	62.4	12.97	89.71	89.73	89.74	0.03
50 µm	90.3	88.1	85.3	5.54	87.62	87.67	87.71	0.09
70 µm	104.3	101.5	99.1	4.98	85.60	85.68	85.69	0.09
95 µm	128.3	128.2	125.5	2.18	82.50	82.52	82.53	0.03

Table 1: Variation in the measured interpad-gap and fill factor with temperature.

We observe that with a decrease in temperature from 25°C to -25°C, the measured interpad-gap decreases by a 2-13 %. However, the change in fill factor value is not significant as it increases by 0.1 %.

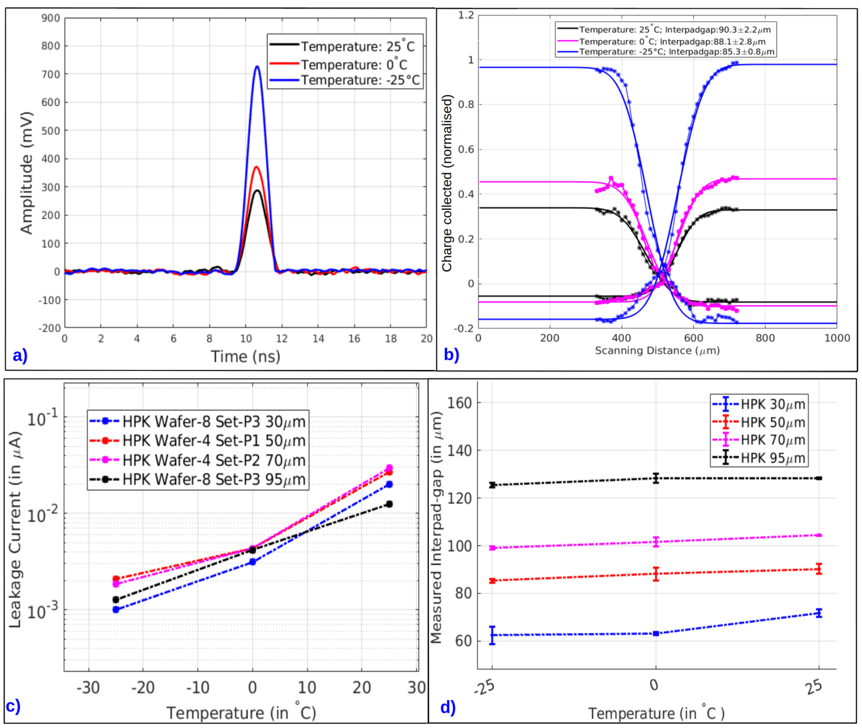

Figure 5: a) Pulse shapes, b) Charge Collected (normalised value) vs scanning distance for sensors (at 25°C, 0°C and -25°C) as the laser scans across two adjacent sensors with 50 µm nominal interpad-gap, c) Leakage current with varying temperature and d) Variation in the measured interpad-gap with temperature. Measurements were performed at a voltage of 180 V.

HPK Sensor (nominal interpad-gap)	Measured interpad-gap of sensor							
	Un-irradiated (in μm)	Irradiated at 5x10^{14} p/cm^2 (in μm)	% decrease	Decrease in Fill factor (in %)	Un-irradiated (in μm)	Irradiated at 5x10^{14} p/cm^2 (in μm)	% decrease	Decrease in Fill factor (in %)
30 µm	68.1	41.4	39.21	0.11	66.0	57.6	1.73	0.11
50 µm	84.8	68.2	19.58	0.39	83.2	70.7	15.02	0.25
70 µm	103.0	84.5	17.96	1.41	101.1	89.8	11.18	0.93
95 µm	117.8	97	17.66	0.80	125.0	-	-	-

Table 2: Variation in the measured interpad-gap and fill factor with proton fluence.

3.2.2. Measured Interpad-gap with varying proton fluence:

The HPK 3.1 production sensors with different nominal interpad-gap values were irradiated with 10 MeV protons at the IBA cyclone 10/5 cyclotron in Department of Chemistry in University of Helsinki [9]. The sensors were placed in a sample holder consisting of collimation slits (of dimensions approximately close to the area of the sensors) such that the integrated current read out from the Keithley 6487 Picoammeter is due to the irradiation of the sensors. The beam profiling was done in such a way that the sample placed under slit 1 and 3 (shown in Figure 5) gets an integrated current of 0.15 µA/cm^2 while sensors under slit 2 and 4 (shown in Figure 5) of the sample holder receive an integrated current of 0.09 µA/cm^2. Four samples were irradiated simultaneously over 1040 s such that samples in 1 and 3 are irradiated with a fluence of 10^{15} protons/cm^2 while 2 and 4 are irradiated with a fluence of 5x10^{14} protons/cm^2. Total integrated current read out from the four slits was 0.42 µA-hr. Note: sensor with 95 µm nominal interpad-gap irradiated at 10^{15} protons/cm^2 underwent breakdown even at low bias voltages.

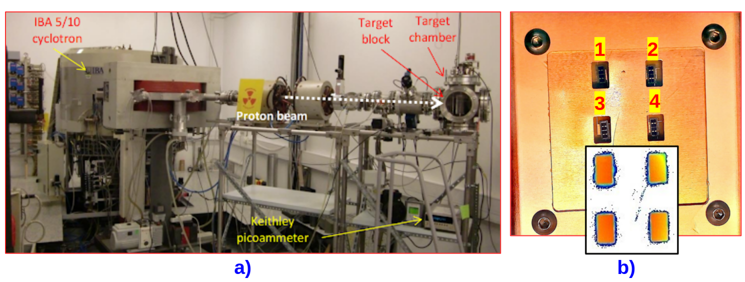

Figure 6: a) IBA 10/5 cyclone cyclotron in the Department of Chemistry, b) Collimator with sample holder showing autoradiograph (using Ag foil) of the beam profile across the four collimation slits.

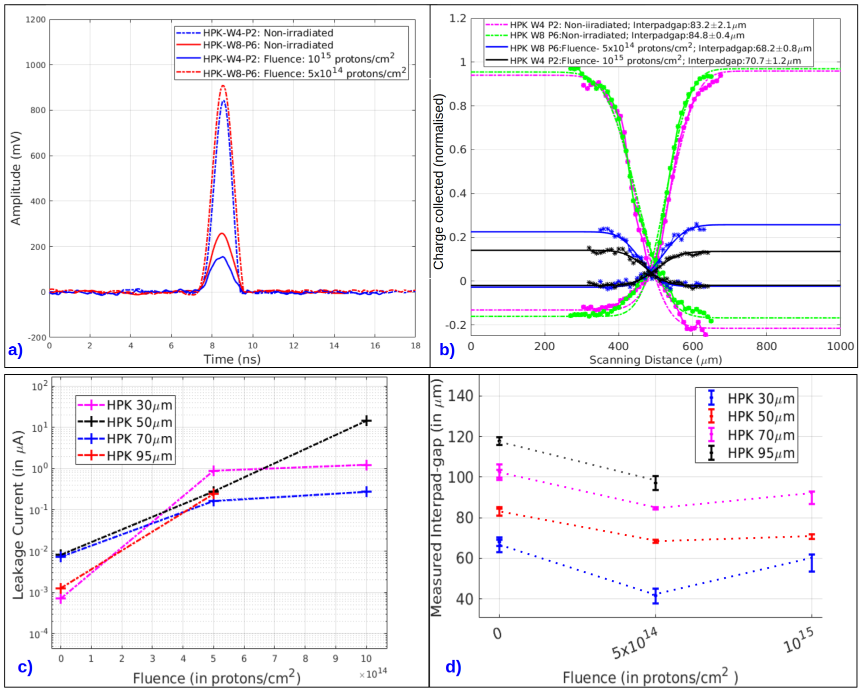

Figure 7: a) Pulse shape of non-irradiated and irradiated samples at different proton fluences and b) Charge Collected (normalised values) vs. scanning distance for sensors as the laser scans across two adjacent pads for sensors with 50 µm interpad-gap. c) Leakage current with varying fluences and d) Variation in the measured interpad-gap with proton fluence for sensors with 30 µm, 50 µm, 70 µm and 95 µm interpad-gap measured at 180 V and temp: -25°C.

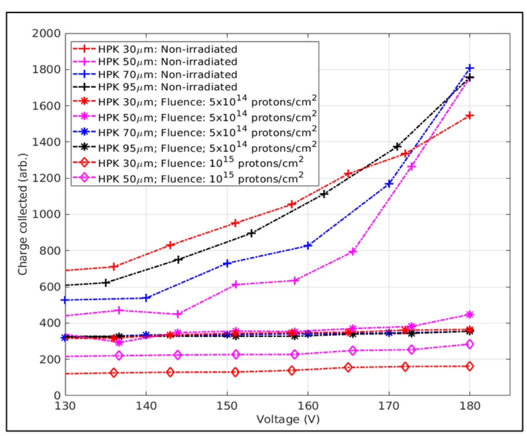

Figure 8: Voltage scans for the non-irradiated and irradiated samples with varying inter-pad gaps measured at -25°C.

The performance of LGADs is affected due to the removal of the acceptor atoms in the gain layer of the device [10]. As a result of which it worsens the time resolution [11] as well as an increase in the leakage current due to the bulk which is unrelated to the gain mechanism [12]. This can be observed in Figure 7c where the leakage current value measured at 180 V at a constant temperature of -25°C, increases by three orders of magnitude with an increase in proton fluence. Further, trapping of charge carriers leads to lower signals (shown in Figure 7a) and hence the degradation of the spatial resolution and the efficiency (as shown in Figure 8) [13, 14].

At a fluence of 5×10^{14} protons/cm^2, interpad-gap is reduced by 20-40% from its value before irradiation and the collected charge decreases by a factor of 3-4 due to trapping of charge carriers causing a degradation in the charge collection efficiency [13]. However, on irradiating the sensors at 10^{15} protons/cm^2, interpad-gap increases in comparison to its value at 5×10^{14} protons/cm^2, since its charge collection efficiency decreases by factor of 6. Therefore, on irradiating the sensors at 10^{15} protons/cm^2, the value of the measured interpad-gap decreases by 11-15% from its value before irradiation. Correspondingly, even though the interpad-gap decreases with an increase in fluence, the fill factor decreases by approximately 1% as the spatial homogeneity is worsened due to the effect of irradiation.

4. Conclusions and summary

The fill factor values for HPK 3.1 production LGADs with different nominal interpad-gap were measured by varying temperature and irradiating them at different proton fluences. The signal waveform as well as the CCE of the detectors were studied by recording 1064 nm wavelength IR-laser induced current transients with a TCT measurements set-up . The measurements were performed at 180 V and low laser intensity. During the measurement campaign four hundred waveforms were recorded at each micron step as the laser scans across adjacent pads of the sensor in order to obtain the measured interpad-gap profile.

Since gain is dependent on temperature, the CCE increases with a decrease in temperature. Our results show that the measured interpad-gap decreases by 2-12 % as the temperature decreases from 25°C to -25°C. However, the fill factor is not affected significantly by changing temperature as its value increases by approximately 0.1%.

Further, the measured interpad-gap decreases on irradiating the sensors at varying proton fluences, Due to acceptor removal of the gain layer, the CCE decreases by a factor of 4–6 with irradiation at high proton fluences. At 10^{15} protons/cm^2, our studies show the measured interpad-gap decreases by 11-15%. However, at the fill factor decreases by 0.1-0.9%. This change is not significantly large. Thus, we conclude that the fill factor does not change significantly with temperature and irradiation at varying proton fluences.

Acknowledgements

The authors are grateful to Dr. Nicolo Cartiglia from Istituto Nazionale di Fisica Nucleare, Universita degli Studi di Torino, Italy and Hamamatsu Photonics K.K, Japan for providing us the sensors for our studies. The authors would like to thank Dr. Eija Tuominen, coordinator of the Detector Laboratory at Helsinki Institute of Physics at the University of Helsinki Department of Physics, for providing the environment for electrical measurements.

References

[1] D. Contardo, M. Klute, J. Mans, L. Silvestris, J. Butler, Technical proposal for the phase-2 upgrade of the cms detector, Tech. Rep. CERN-LHCC-2015-010. LHCC-P-008. CMS-TDR-15-02, CERN, Geneva (Jun 2015).
URL https://cds.cern.ch/record/2020886

[2] C. CMS, A MIP Timing Detector for the CMS Phase-2 Upgrade, Tech. Rep. CERN-LHCC-2019-003. CMS-TDR-020, CERN, Geneva (Mar 2019).
URL https://cds.cern.ch/record/2667167

[3] C. Collaboration, TECHNICAL PROPOSAL FOR A MIP TIMING DETECTOR IN THE CMS EXPERIMENT PHASE 2 UPGRADE, Tech. Rep. CERN-LHCC-2017-027. LHCC-P-009, CERN, Geneva, this document describes a MIP timing detector for the Phase-2 upgrade of the CMS experiment, in view of HL-LHC running (Dec 2017).
URL https://cds.cern.ch/record/2296612

[4] C. Pena, Precision timing with the cms mip timing detector, Tech. Rep. CMS-CR-2018-168, CERN, Geneva (Aug 2018).
URL https://cds.cern.ch/record/2639962

[5] Particulars, advanced measurement systems, http://particulars.si/index.php, accessed: January, 2018 (2018).

[6] C. R. Crowell, S. M. Sze, Temperature dependence of avalanche multiplication in semiconductors, Applied Physics Letters 9 (6) (1966) 242–244 (1966).

arXiv:https://doi.org/10.1063/1.1754731, doi:10.1063/1.1754731. URL https://doi.org/10.1063/1.1754731

[7] V. Sola, R. Arcidiacono, A. Bellora, et al., Ultra-Fast Silicon Detectors for 4D tracking, Journal of Instrumentation 12 (02) (2017) C02072–C02072 (feb 2017). doi:10.1088/1748-0221/12/02/c02072.

[8] R. Mulargia, Temperature dependence of the response of ultra fast silicon detectors, Journal of Instrumentation 11 (12) (2016) C12013–C12013 (dec 2016). doi:10.1088/1748-0221/11/12/c12013.

[9] K. Helariutta, et al., The radiochemistry cyclotron in University of Helsinki, Nukleonika 48(suppl2) (2003) S173–S174 (01 2003).

[10] G. Kramberger, et al., Radiation effects in Low Gain Avalanche Detectors after hadron irradiations, Journal of Instrumentation 10 (07) (2015) P07006–P07006 (jul 2015). doi:10.1088/1748-0221/10/07/p07006.

[11] M. Ferrero, Radiation resistant LGAD design, Nuclear Instruments and Methods in Physics Research Section A: Accelerators, Spectrometers, Detectors and Associated Equipment 919 (2019) 16 – 26 (2019). doi:https://doi.org/10.1016/j.nima.2018.11.121. URL http://www.sciencedirect.com/science/article/pii/S0168900218317741

[12] Z. Galloway, V. Fadeyev, et al., Properties of HPK UFSD after neutron irradiation up to 6e15 n/cm^2, Nuclear Instruments and Methods in Physics Research Section A: Accelerators, Spectrometers, Detectors and Associated Equipment 940 (2019) 19 – 29 (2019). doi:https://doi.org/10.1016/j.nima.2019.05.017. URL http://www.sciencedirect.com/science/article/pii/S0168900219306278

[13] M. Moll, Radiation damage in silicon particle detectors: Microscopic defects and macroscopic properties, Ph.D. thesis, Hamburg U. (1999). URL http://www-library.desy.de/cgi-bin/showprep.pl?desy-thesis99-040

[14] W. Adam, T. Bergauer, et al., Trapping in proton irradiated p$^+$-n-n$^+$ silicon sensors at fluences anticipated at the HL-LHC outer tracker, Journal of Instrumentation 11 (04) (2016) P04023–P04023 (apr 2016). doi:10.1088/1748-0221/11/04/p04023.